Biot-Rayleigh theory of wave propagation in double-porosity media

J. Ba,[1] J. M. Carcione,[2] and J. X. Nie[3]

[1]   We derive the equations of motion of a double-porosity medium based on Biot's theory of poroelasticity and on a generalization of Rayleigh's theory of fluid collapse to the porous case. Spherical inclusions are imbedded in an unbounded host medium having different porosity, permeability, and compressibility. Wave propagation induces local fluid flow between the inclusions and the host medium because of their dissimilar compressibilities. Following Biot's approach, Lagrange's equations are obtained on the basis of the strain and kinetic energies. In particular, the kinetic energy and the dissipation function associated with the local fluid flow motion are described by a generalization of Rayleigh's theory of liquid collapse of a spherical cavity. We obtain explicit expressions of the six stiffnesses and five density coefficients involved in the equations of motion by performing "gedanken" experiments. A plane wave analysis yields four wave modes, namely, the fast P and S waves and two slow P waves. As an example, we consider a sandstone and compute the phase velocity and quality factor as a function of frequency, which illustrate the effects of the mesoscopic loss mechanism due to wave-induced fluid flow.

1.   Introduction

[2]   The mechanism of local fluid flow (LFF) explains the high attenuation of low-frequency elastic waves in fluid-saturated rocks. When seismic waves propagate through small-scale heterogeneities, pressure gradients are induced between regions of dissimilar properties. *Pride et al.* [2004] have shown that attenuation and velocity dispersion measurements can be explained by the combined effect of mesoscopic-scale inhomogeneities and energy transfer between wave modes. We refer to this mechanism as mesoscopic loss. The mesoscopic-scale length is intended to be larger than the grain sizes, but much smaller than the wavelength of the pulse. For instance, if the matrix porosity varies significantly from point to point, diffusion of pore fluid between different regions constitutes a mechanism that can be important at seismic frequencies. Reviews of the different theories and authors, who have contributed to the understanding of this mechanism, are given by, for instance, *Carcione and Picotti* [2006] and *Carcione* [2007].

[3]   An attempt to introduce squirt flow effects is presented by *Dvorkin et al.* [1995], in which a force applied to the area of contact between two grains produces a displacement of the surrounding fluid in and out of this area. Since the fluid is viscous, the motion is not instantaneous and energy dissipation occurs. However, this mechanism cannot explain the attenuation in the seismic band [*Pride et al.*, 2004].

[4]   *White* [1975] and *White et al.* [1975] were the first to introduce the mesoscopic loss mechanism based on approximations in the framework of Biot theory. They considered gas pockets in a water-saturated porous medium and porous layers alternately saturated with water and gas, respectively. These are the first so-called "patchy saturation" models. *Dutta and Odé* [1979a, 1979b] solved the problem exactly using Biot theory and confirmed White's results. The mesoscopic loss theory has been further refined by *Gurevich et al.* [1997], *Shapiro and Müller* [1999], *Johnson* [2001], *Müller and Gurevich* [2004] and *Pride et al.* [2004]. *Miksis* [1988] included the dissipation due to contact line movement to describe the attenuation of seismic waves in a partially saturated rock. *Gurevich et al.* [1997] obtained the P wave quality factor as a function of frequency for 1D finely layered poroelastic media (normal to layering). They considered Biot's loss, scattering and mesoscopic flow loss, and found that the quality factor is approximately given by the harmonic average of the corresponding single quality factors. *Shapiro and Müller* [1999] reinterpreted the role of the hydraulic permeability in the mesoscopic flow mechanism, concluding that this permeability corresponds to the zero-frequency limit of

[1]Research Institute of Petroleum Exploration and Development, PetroChina, Beijing, China.
[2]Istituto Nazionale di Oceanografia e di Geofisica Sperimentale, Trieste, Italy.
[3]State Key Laboratory of Exploration Science and Technology, Beijing Institute of Technology, Beijing, China.

the seismic permeability actually controlling the loss. *Müller and Gurevich* [2004] performed numerical experiments in random and periodic media with patchy saturation (gas and water) with a correlation length of 20 cm, showing attenuation peaks in the seismic band and at 80 % water saturation. *Brajanovski et al.* [2006] analyzed compressional wave attenuation in fractured porous media and derived the characteristic frequency which yield estimates of permeabilities and thicknesses of the rock fracture system.

[5] *Johnson* [2001] developed a generalization of White model for patches of arbitrary shape. This model has two geometrical parameters, besides the usual parameters of Biot theory: the specific surface area and the size of the patches. Patchy saturation effects on acoustic properties have been observed by *Murphy* [1982] and *Knight and Nolen-Hoeksema* [1990]. *Cadoret at al.* [1995] investigated the phenomenon in the laboratory at the frequency range 1–500 kHz. Two different saturation methods result in different fluid distributions and produce two different values of velocity for the same saturation. Imbibition by depressurization produces a very homogeneous saturation, while drainage by drying produces heterogeneous saturations at high water saturation levels. In the latter case, the experiments show considerably higher velocities, as predicted by White model.

[6] *Carcione et al.* [2003] performed numerical-modeling experiments based on Biot's equations of poroelasticity and White model of regularly distributed spherical gas inclusions. Fractal models, such as the von Kármán correlation function, calibrated by the CT scans, were used by *Helle et al.* [2003] to model heterogeneous rock properties and perform numerical experiments based on Biot's equations of poroelasticity.

[7] Generalization of Biot's theory to composite and double-porosity media is generally based on Biot's energy approach using Lagrange's equations [*Biot*, 1962]. A generalization of Biot's theory for two porous frames is given by *Carcione et al.* [2000]. *Carcione and Seriani* [2001] developed a numerical algorithm for simulation of wave propagation in frozen porous media, where the pore space is filled with ice and water. The model, based on a Biot-type three-phase theory obtained from first principles, predicts three P waves (one fast P wave and two slow P waves) and two S waves in the high-frequency limit and the corresponding diffusive modes at low frequencies. Attenuation is modeled with Zener relaxation functions which allow a differential formulation based on memory variables. The generalization of these differential equations to the variable porosity case is given by *Carcione et al.* [2003], by using the analogy with the two-phase case and the complementary energy theorem. A more rigorous generalization is given by *Santos et al.* [2004]. In this way it is possible to simulate propagation in a frozen porous medium with fractal variations of porosity, in which solid substrate, ice, and water coexist and the two solid phases are weakly coupled. A generalization of the splitting method to the three-phase case is performed to solve these equations.

[8] The simulation of two slow waves due to capillary forces in a partially saturated porous medium is presented by *Carcione et al.* [2004], based on the theory developed by *Santos et al.* [1990a, 1990b]. The pores are filled with a wetting fluid and a nonwetting fluid, and the model, based on a Biot-type three-phase theory, predicts three P waves and one S wave. Again, realistic attenuation is modeled with exponential relaxation functions and memory variables. Surface tension effects in the fluids, which are not considered in the classical Biot theory, cause the presence of a second slow wave, which is faster than the classical Biot slow wave.

[9] *Berryman and Wang* [2000] presented phenomenological equations for the poroelastic behavior of a double-porosity medium to account for storage porosity and fracture porosity in oil and gas reservoirs. A recent Biot-type poroelastic theory treats the mesoscopic loss created by lithological patches having, for example, different degrees of consolidation [*Pride et al.*, 2004]. There are two phases with dissimilar porosity and the theory explicitly considers the field variables of these phases (see Figure 1). *Ba et al.* [2008a, 2008b] have solved the governing equations (homogeneous case) and simulated the wavefields using the pseudospectral method. *Liu et al.* [2009] solved equivalent poroviscoacoustic equations by approximating the mesoscopic complex moduli in the frequency domain by using Zener mechanical models, in the same way as *Carcione* [1998] represented the Biot loss mechanism. The equations are then solved in the time domain using memory variables and the splitting method. *Agersborg et al.* [2009] used the T matrix approach to illustrate the effects of LFF in double-porosity carbonates, and a relaxation time is used as an empirical parameter dependent on the scale of the pores and cracks.

[10] Wave-induced LFF in mesoscopic heterogeneous rocks is capable of explaining the measured level of wave dispersion and attenuation in the seismic band (1–10^4 Hz). The theory presented here have been developed from first physical principles. All parameters can be measured or estimated from measurements. The flow dynamics is based on Rayleigh's theory [*Rayleigh*, 1917], which describes the collapse of a spherical cavity in a liquid. Rayleigh assumed an incompressible fluid so that the whole motion is determined by the sphere boundary. *Lamb* [1923] analyzed the early stages of a submarine explosion on the basis of Rayleigh's theory. The governing equation [*Lamb*, 1923, equation (30)] describes periodic spherical vibrations, which can be applied to model the local flow process of a spherical inclusion. Similar oscillatory motions were studied by *Vokurka* [1985a, 1985b].

[11] To describe wave-induced LFF, we consider two types of pores of different compressibility; that is, LFF occurs between soft pores and stiff pores. We propose this double-porosity approach by using a generalization of Rayleigh's theory of liquid collapse of a spherical cavity in the framework of *Biot*'s [1962] energy approach. For the purpose of quantitatively describing the dynamic process of wave-induced LFF in heterogeneous fluid/solid composites, we derive the dynamic governing equation from first principles. First, we give the kinetic energy expression for LFF by considering the model of a sphere inclusion being imbedded in a uniform porous host medium. Second, we substitute the kinetic energy and strain potential energy function into Lagrange equations, and derive three dynamic governing
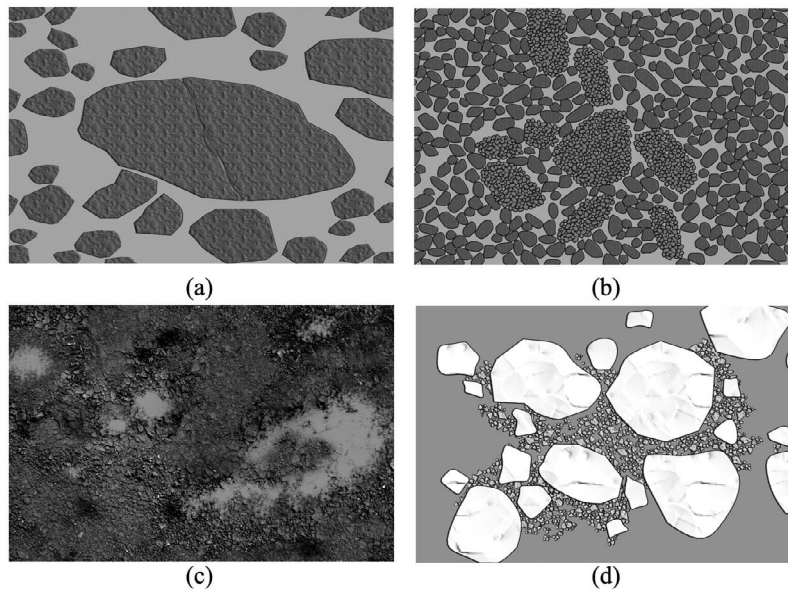
Figure 1. Synoptic diagram for four types of double-porosity medium in nature. (a) Flat throats connected to stiff pores in microscopic scale. (b) Patches of small grains embedded in a matrix formed of large grains. (c) Strongly dissolved dolomite, in which powder crystals are present in the pores forming a second matrix. (d) Partially melted ice matrix, whose pores are filled with a mixture of loosely contacted micro-ice crystals and water.

equations for wave propagation and the one governing equation for LFF. We then obtain the relevant stiffness coefficients by performing "gedanken experiments" and compute plane wave solutions, to obtain the phase velocity and quality factor as a function of frequency.

2. Strain Energy

[12] We consider the inclusion model shown in Figure 2, with the following assumptions: (1) The inclusions are spherical and homogeneous and have the same size; (2) the boundary conditions between the inclusions and the host medium are open; (3) the radius is much smaller than the wavelength; and (4) the inclusion volume ratio is low, so we neglect interactions between inclusions. The fluid variation can be evaluated as follows. Assume that R_0 is the radius of the (spherical) inclusion at rest, and R is the dynamic radius of the fluid sphere after the LFF process (see Figure 2), which is a function of time. The connections between inclusions and host medium are assumed to be completely connected [*Deresiewicz and Skalak*, 1963]. In actual rocks, there may be partial connection or no connection between different components.

[13] Let us denote the time variable by t and the spatial variables by x_i, $i = 1, 2, 3$, the displacement vector of the solid matrix by $\mathbf{u} = (u_1, u_2, u_3)^T$ and the components of the average fluid displacement vector in the two porosity systems (host medium and inclusions) as $\mathbf{U}^{(m)} = (U_1^{(m)}, U_2^{(m)}, U_3^{(m)})^T$, $m = 1, 2$, respectively. (In a double-porosity medium, the difference between the fluid displacement in the inclusion and in the host medium is much larger than that of the solid phase, due to the fluid lower bulk modulus. In this context, we consider one solid displacement vector and two

fluid displacement vectors [*Pride et al.*, 2004].) Moreover, we introduce the corresponding strain components:

$$e_{ij} = \frac{1}{2}\left(\partial_j u_i + \partial_i u_j\right) \quad \text{and} \quad \xi_{ij}^{(m)} = \frac{1}{2}\left(\partial_j U_i^{(m)} + \partial_i U_j^{(m)}\right), \quad (1)$$

and define the dilatations as

$$e = e_{ii} = \partial_i u_i \quad \text{and} \quad \xi_m = \xi_{ii}^{(m)} = \partial_i U_i^{(m)}, \quad (2)$$

where ∂_i denotes a partial derivative with respect to the spatial variable x_i and the Einstein summation of repeated indices is
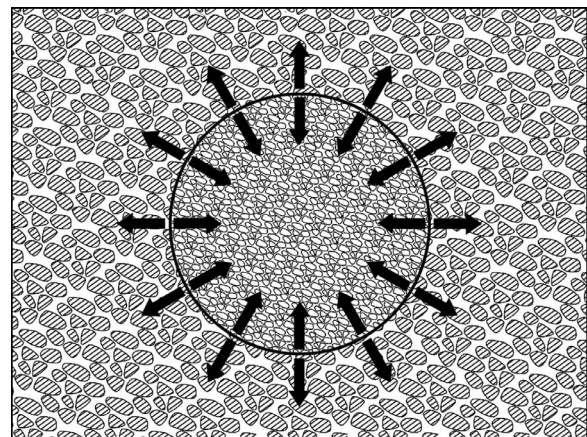

Figure 2. A fluid sphere's swell-shrinking vibration between the inclusion and the host medium under elastic wave excitation.

assumed. The strain energy in double-porosity medium is a function of five independent variables,

$$W = W(I_1, I_2, I_3, \xi_1, \xi_2), \qquad (3)$$

where

$$I_1 = e_{ii}, \quad I_2 = \begin{vmatrix} e_{11} & e_{12} \\ e_{12} & e_{22} \end{vmatrix} + \begin{vmatrix} e_{22} & e_{23} \\ e_{23} & e_{33} \end{vmatrix} + \begin{vmatrix} e_{33} & e_{13} \\ e_{13} & e_{11} \end{vmatrix} \quad \text{and}$$

$$I_3 = \begin{vmatrix} e_{11} & e_{12} & e_{13} \\ e_{12} & e_{22} & e_{23} \\ e_{13} & e_{23} & e_{33} \end{vmatrix}. \qquad (4)$$

We consider a Taylor expansion of W and neglect all terms whose orders are higher than two,

$$2W = (A + 2N)I_1^2 - 4NI_2 + 2Q_1 I_1 \xi_1 + R_1 \xi_1^2$$
$$+ 2Q_2 I_1 \xi_2 + R_2 \xi_2^2, \qquad (5)$$

where A, N, Q_1, R_1, Q_2 and R_2 are stiffnesses.

[14] We use a scalar ζ to denote the fluid body strain's increment in the LFF process generated by the passage of a wave. There is an internal vibration process accompanying wave's propagation, which causes rock to be relaxed. The deformation of pore fluid in the two types of pores is rebalanced before potential energy is transferred to kinetic energy.

$$2W = (A + 2N)I_1^2 - 4NI_2 + 2Q_1 I_1 (\xi_1 + \phi_2 \zeta) + R_1 (\xi_1 + \phi_2 \zeta)^2$$
$$+ 2Q_2 I_1 (\xi_2 - \phi_1 \zeta) + R_2 (\xi_2 - \phi_1 \zeta)^2, \qquad (6)$$

where ϕ_m are the porosities.

[15] Then, the LFF interaction is represented by the fluid variation ζ. Fluid flow from $m = 1$ to $m = 2$ implies the fluid variation $-\phi_1 \zeta$, where the minus sign is a convention. The opposite flow induces the variation $\phi_2 \zeta$ in system 1, such that the conservation of fluid mass is satisfied, i.e., $\phi_1(\phi_2 \zeta) + \phi_2(-\phi_1 \zeta) = 0$.

[16] Based on the model shown in Figure 2, we then have that the effective fluid volume variation in system 1 is $\phi_1 \zeta \approx 1 - V_0/V$, where V_0 and V are the volumes of the fluid sphere corresponding to the radius of inclusion R_0 and the dynamic radius of fluid sphere R, respectively. Then

$$\zeta = \frac{1}{\phi_1}\left(1 - \frac{R_0^3}{R^3}\right). \qquad (7)$$

As we shall see later, the LFF terms are responsible for wave attenuation.

3. Kinetic Energy

[17] Let us denote by v_m, $m = 1$, 2 the volume fraction of phase m present in an averaging volume. The total porosity is given by

$$\phi = \phi_1 + \phi_2, \qquad (8)$$

where

$$\phi_m = v_m \phi_{m0}, \qquad (9)$$

where ϕ_{m0} is the porosity in each phase.

[18] *Berryman and Wang* [2000] generalized Biot's kinetic energy expression [*Biot*, 1956] to the double-porosity case. Their kinetic energy is a function of the fluid particle velocity. In this work, we start from Biot's theory [*Biot*, 1962], where the kinetic energy is a function of the fluid particle velocity relative to the solid phase. Generalizing Biot's kinetic energy T to the double-porosity case, we have

$$2T = \rho_0 \sum_i \dot{u}_i^2 + \rho_f \sum_m \int_{\Omega_m} \sum_i \left(\dot{u}_i + g_i^{(m)} + l_i^{(m)}\right)^2 d\Omega_m, \qquad (10)$$

where $\mathbf{g}^{(m)} = (g_1, g_2, g_3)^\top$ and $\mathbf{l}^{(m)} = (l_1, l_2, l_3)^\top$ denote the relative microvelocity fields of the fluid in each system, associated with the global and local flows, respectively, Ω_m is the pore volume, and

$$\rho_0 = (1 - \phi)\rho_s, \qquad (11)$$

with ρ_s and ρ_f the solid and fluid mass densities, respectively. The symbols Σ_i and Σ_m denote summation from 1 to 3 corresponding to the Cartesian coordinates and summation from 1 to 2 corresponding to the two porosity systems, and a dot above a variable indicate time differentiation.

[19] Let us consider the integral

$$\rho_f \int_{\Omega_m} \left(\dot{u}_i + g_i^{(m)} + l_i^{(m)}\right)^2 d\Omega_m \qquad (12)$$

and analyze the different terms. First,

$$\rho_f \int_{\Omega_m} \dot{u}_i^2 d\Omega_m = \rho_m \dot{u}_i^2, \quad \rho_m = \phi_m \rho_f. \qquad (13)$$

Second,

$$\rho_f \int_{\Omega_m} \dot{u}_i g_i^{(m)} d\Omega_m = \rho_f \dot{u}_i \dot{w}_i^{(m)}, \qquad (14)$$

where

$$w_i^{(m)} = \phi_m \left(U_i^{(m)} - u_i\right) \qquad (15)$$

is the macroscopic particle velocity of the fluid relative to the solid [*Biot*, 1962]. We also have

$$\rho_f \int_{\Omega_m} \dot{u}_i l_i^{(m)} d\Omega_m = \rho_f \dot{u}_i \int_{\Omega_m} l_i^{(m)} d\Omega_m = 0, \qquad (16)$$

(see Appendix A), since the flow vector is perpendicular to the surface of the inclusion if we assume that seismic wavelength is much larger than the inclusion size, the inclusion is spherical and each component (inclusions or host medium) can be regarded as a homogeneous single-porosity medium (see Figure 2). Moreover,

$$\int_{\Omega_m} g_i^{(m)} l_i^{(m)} d\Omega_m = 0 \qquad (17)$$

for compressional waves (see Appendix A), because the inclusion is spherical and assumed uniform, and in this case, $g_i^{(m)}$ has the same value at two opposite points relative to the

center of the sphere, while $l_i^{(m)}$ have the same absolute value but different sign.

[20] Using the preceding equations, the kinetic energy (10) becomes

$$2T = \rho \sum_i \left(\dot{u}_i^2 + 2\rho_f \sum_m \dot{u}_i \dot{w}_i^{(m)} \right) + \rho_f \sum_m \int_{\Omega_m} \sum_i \left[\left(g_i^{(m)}\right)^2 + \left(l_i^{(m)}\right)^2 \right] d\Omega_m,$$
(18)

where

$$\rho = \rho_0 + \rho_1 + \rho_2.$$
(19)

With the assumption of an isotropic microvelocity field, isolating the terms involving local fluid flow terms from the others, equation (18) reduces to

$$2T = \rho \sum_i \left(\dot{u}_i^2 + 2\rho_f \sum_m \dot{u}_i \dot{w}_i^{(m)} \right) + \sum_m \overline{\rho}_m \sum_i \left(\dot{w}_i^{(m)} \right)^2 + 2T_L,$$
(20)

where $\overline{\rho}_m$, $m = 1, 2$ are Biot mass coefficients (see equation (44) and *Biot* [1962], *Carcione et al.* [2000], and *Carcione* [2007]) and

$$2T_L = \rho_f \sum_m \int_{\Omega_m} \sum_i \left(l_i^{(m)}\right)^2 d\Omega_m$$
(21)

is the LFF kinetic energy density related to compressional deformations, as shown in Figure 2. Since T_L does not depend on vectors $\mathbf{u}$ and $\mathbf{w}^{(m)}$, we may evaluate it independently as shown later. We may rewrite the kinetic energy in terms of vectors $\mathbf{U}^{(m)}$ as

$$2T = \rho_{00} \sum_i \dot{u}_i^2 + 2 \sum_m \rho_{0m} \sum_i \dot{u}_i \dot{U}_i^{(m)} + \sum_m \rho_{mm} \sum_i \left(\dot{U}_i^{(m)} \right)^2 + 2T_L,$$
(22)

where

$$\begin{aligned} \rho_{00} &= \rho - \sum_m \phi_m \left(2\rho_f - \overline{\rho}_m \phi_m\right), \\ \rho_{mm} &= \overline{\rho}_m \phi_m^2, \\ \rho_{0m} &= \rho_m - \rho_{mm}. \end{aligned}$$
(23)

4. Mesoscopic Loss and the Rayleigh Model

[21] In this section, we analyze the kinetic energy of the LFF process and establish a relation between fluid sphere's dynamic radius and fluid increment. Let R be the dynamic radius of the fluid sphere, $\dot{R}$ the particle velocity at the boundary, $r > R$, and $\dot{r}$ the particle velocity outside the inclusion, such that these particle velocities are the radial component of vector $\mathbf{U}$. Since in our system there is a matrix (skeleton), we generalize Rayleigh's theory to the case of a porous medium.

[22] In the first step of this simple generalization, the boundary condition at the surface of the inclusion is the continuity of vector $\dot{\mathbf{w}}$ defined in equation (15), or $\phi_{10}\dot{r} = \phi_{20}\dot{R}$. Second, Rayleigh's equation (1), which expresses the

conservation of fluid flow (in our case, between the host medium and the inclusion) can be generalized as

$$4\pi R^2 \dot{R} \phi_{20} = 4\pi r^2 \dot{r} \phi_{10}, \quad \text{or} \quad \frac{\dot{r}}{R} = \frac{R^2 \phi_{20}}{r^2 \phi_{10}},$$
(24)

which satisfies the boundary condition at $r = R$. Third, following *Rayleigh* [1917], the kinetic energy outside the inclusion is then

$$T_1 = \frac{1}{2} \phi_{10} \rho_f \int_R^\infty 4\pi r^2 \dot{r}^2 dr,$$
(25)

where T_1 gives the kinetic energy of a single inclusion. Substituting equation (24) gives

$$T_1 = 2\pi \rho_f R^3 \dot{R}^2 \left(\phi_{20}^2 / \phi_{10}\right).$$
(26)

[23] The volume ratio of the inclusion is $v_2 = (4/3)\pi R^3 N_0 \approx (4/3)\pi R_3 N_0$, where N_0 is the number of inclusions per unit volume of composite. Using equation (9), we have

$$R^3 = \frac{3\phi_2}{4\pi\phi_{20}N_0}.$$
(27)

Using this equation, multiplying (26) by N_0, and since from equation (7) it is

$$\dot{R} \approx \frac{1}{3} \phi_1 R_0 \dot{\zeta},$$
(28)

which is a relation between dynamic radius and fluid increment, we obtain the kinetic energy density for all the inclusions,

$$T_L = \frac{1}{6} \left(\frac{\phi_1^2 \phi_2 \phi_{20}}{\phi_{10}} \right) \rho_f R_0^2 \dot{\zeta}^2.$$
(29)

Here we assume the volume ratio of inclusions is low and the distance between two inclusions is large enough, so that we can neglect the interaction between the different inclusions. The macroscopic average approximation is used for double-porosity composites, which is similar to the effective medium theory of multiphase composites [*Berryman and Berge*, 1996]. When the effective medium theory is considered to be a low concentration approximation based on "noninteraction" assumptions by *Kuster and Toksoz* [1974], it is found to be acceptable for inclusion volume ratios lower than 0.2 [*Wilkens et al.*, 1991].

[24] Wave scattering in solid matrix and LFF can happen simultaneously in the fluid-saturated double-porosity system. Nevertheless, the scattering effect is much weaker than the fluid's swell-shrinking motion, since the scattering peak is away from the frequency band under consideration. In this work, the scattering in solid matrix is neglected. A similar approximation was also used in previous studies [*Dvorkin and Nur*, 1993; *Pride et al.*, 2004].

5. Dissipation Function

[25] The generalization of Biot's dissipation function, D [*Biot*, 1962; *Carcione*, 2007], to the present case is

$$2D = \sum_m b_m \mathbf{w}^{(m)} \cdot \mathbf{w}^{(m)},$$
(30)

where $\mathbf{w}^{(m)}$ is defined in equation (15), and

$$b_m = v_m \phi_{m0}^2 \left(\frac{\eta}{\kappa_m} \right) = \phi_m \phi_{m0} \left(\frac{\eta}{\kappa_m} \right), \tag{31}$$

where η is the viscosity and κ_m is the permeability of the host medium ($m = 1$) and inclusion ($m = 2$).

[26] Similar to the calculation of the kinetic energy T_L (see equation (25)), the dissipation function of the LFF process is obtained as

$$D_L = \frac{1}{2} \phi_{10}^2 \left(\frac{\eta}{\kappa_1} \right) \int_R^\infty 4\pi r^2 \dot{r}^2 dr = 2\pi \phi_{20}^2 \left(\frac{\eta}{\kappa_1} \right) R^3 \dot{R}^2, \tag{32}$$

where we have used equation (24). Moreover, we have to divide D_L by the volume of the inclusion to obtain the dissipation function per unit volume. Finally, using equations (27) and (28), we obtain

$$D_L = \frac{3}{2} \frac{\eta \phi_2 \phi_{20}}{\kappa_1} \dot{R}^2 = \frac{1}{6} \left(\frac{\eta}{\kappa_1} \right) \phi_1^2 \phi_2 \phi_{20} R_0^2 \dot{\zeta}^2. \tag{33}$$

6. Stress-Strain Relation and Determination of the Stiffness and Density Coefficients

[27] *Johnson* [1986] performed three "gedanken" experiments and derived the explicit expressions for the four Biot elastic constants of a single-porosity medium. Here, similar experiments are discussed for a double-porosity medium. First of all, we derive the stress-strain relations for the solid and fluid phases of as

$$\tau_{ij} = \frac{\partial W}{\partial e_{ij}} \quad \text{and} \quad \tau^{(m)} = \frac{\partial W}{\partial \xi_m}, \quad m = 1, 2. \tag{34}$$

Neglecting the LFF process, we obtain

$$\tau_{ij} = \left(Ae + \sum_m Q_m \xi_m \right) \delta_{ij} + 2N e_{ij}, \\ \tau^{(m)} = Q_m e + R_m \xi_m, \tag{35}$$

where δ_{ij} is Kronecker's delta.

[28] Let us perform the three idealized experiments [*Biot and Willis*, 1957; *Johnson*, 1986; *Carcione*, 2007].

[29] 1. The material is subjected to a pure shear deformation ($e = \xi_m = 0$). In this case, it is clear that N is the shear modulus of the frame, since the fluid does not contribute to the shearing force. Let us denote

$$N = \mu_b \tag{36}$$

as the dry rock shear modulus.

[30] 2. The rock sample is surrounded by a flexible rubber jacket, subjected to a hydrostatic pressure p_0, and the pore fluid is allowed to flow in and out. Only the skeleton affects the rock deformation. Then $\tau_{ij} = -p_0 \delta_{ij}$ and $e = \text{div} \cdot \mathbf{u} = -p_0/K_b$, where K_b is the frame modulus, while the pore fluid remains unloaded ($\tau^{(m)} = 0$). Substituting these relations into equation (35) gives

$$A + \frac{2}{3} N - \sum_m \frac{Q_m^2}{R_m} = K_b. \tag{37}$$

[31] 3. The rock sample is subjected to a uniform hydrostatic pressure p_1 and the mineral grain is homogeneous and isotropic. We have $\tau_{ij} = -(1 - \phi)p_1 \delta_{ij}$, where $\phi = \phi_1 + \phi_2$, $\tau^{(m)} = -\phi_m p_1$, $e = -p_1/K_s$, $\xi_m = -p_1/K_f$, where K_s and K_f are the solid and fluid bulk moduli, respectively. Then, another three relations are derived from equation (35),

$$\frac{A + 2N/3}{K_s} + \frac{\sum_m Q_m}{K_f} = 1 - \phi, \\ \frac{Q_m}{K_s} + \frac{R_m}{K_f} = \phi_m, \quad m = 1, 2. \tag{38}$$

[32] One more relation is necessary to obtain the coefficients since there are four equations and five unknowns. Let us consider the second experiment, where the fluid pressures vanish. If we consider each single phase isolated from the other, we have $Q_{m0} e_m + R_{m0} \xi_m = 0$, where the elastic constants are those given by the single-porosity Biot's theory [*Carcione*, 2007; equations (7.17) and (7.31)], i.e., $Q_{m0}/R_{m0} = \alpha_m/\phi_{m0} - 1$, where $\alpha_m = 1 - K_{bm}/K_s$ is the Biot-Willis coefficient. Since $e_m K_{bm} = -p_0$, we have

$$\frac{\xi_1}{\xi_2} = \frac{Q_{10} R_{20} K_{b2}}{Q_{20} R_{10} K_{b1}} = \frac{\phi_{20} K_{b2}}{\phi_{10} K_{b1}} \left(\frac{\alpha_1 - \phi_{10}}{\alpha_2 - \phi_{20}} \right). \tag{39}$$

Approximating the dilatation ratio ξ_1/ξ_2 of the composite (see (35)) by (39), yields

$$\frac{\xi_1}{\xi_2} = \frac{Q_1 R_2}{Q_2 R_1} \approx \frac{\phi_{20}}{\phi_{10}} \left[\frac{1 - (1 - \phi_{10})K_s/K_{b1}}{1 - (1 - \phi_{20})K_s/K_{b2}} \right] \equiv \beta. \tag{40}$$

Thus, $\beta = Q_1 R_2/(Q_2 R_1)$ is the additional equation, with β given by (40).

[33] Using the preceding equations we find the expressions of the stiffness coefficients:

$$A = (1 - \phi)K_s - \frac{2}{3} N - \frac{K_s}{K_f}(Q_1 + Q_2), \\ Q_1 = \frac{\beta \phi_1 K_s}{\beta + \gamma}, \qquad Q_2 = \frac{\phi_2 K_s}{1 + \gamma}, \\ R_1 = \frac{\phi_1 K_f}{\beta/\gamma + 1}, \qquad R_2 = \frac{\phi_2 K_f}{1/\gamma + 1}, \\ \gamma = \frac{K_s}{K_f} \left(\frac{\beta \phi_1 + \phi_2}{1 - \phi - K_b/K_s} \right). \tag{41}$$

[34] On the other hand, the calculations of the density coefficients follows *Biot* [1956]. We have

$$(1 - \phi)\rho_s = \rho_{00} + \sum_m \rho_{0m}, \\ \phi_m \rho_f = \rho_{0m} + \rho_{mm}, \quad m = 1, 2. \tag{42}$$

In terms of the tortuosity, $\mathcal{T}_m$, we have

$$\rho_{mm} = v_m \mathcal{T}_m \phi_{m0} \rho_f = \mathcal{T}_m \phi_m \rho_f, \tag{43}$$

such that

$$\bar{\rho}_m = \frac{\mathcal{T}_m \rho_f}{\phi_m}. \tag{44}$$

Following *Berryman* [1979],

$$\mathcal{T}_m = \frac{1}{2} \left(1 + \frac{1}{\phi_{m0}} \right). \tag{45}$$

Finally,

$$2\rho_{00} = 2(1 - \phi)\rho_s - (\phi - 1)\rho_f,$$
$$2\rho_{0m} = (\phi_m - v_m)\rho_f, \tag{46}$$
$$2\rho_{mm} = (\phi_m + v_m)\rho_f.$$

7. Lagrange's Equations and Equations of Motion

[35] The equation of motion can be obtained from Hamilton's principle. The Lagrangian density of a conservative system is defined as

$$L = T - W. \tag{47}$$

The motion of a conservative system can be described by Lagrange's equation, which is based on Hamilton's principle of least action [*Achenbach*, 1984, p. 61]. Substituting kinetic energy expressions, potential energy expressions and dissipation functions into Lagrange equation, the motion equations in double-porosity medium can be derived. Lagrange's equations, with the displacements as generalized coordinates, can be written as

$$\partial_t\left(\frac{\partial L}{\partial \dot{u}}\right) + \partial_j\left[\frac{\partial L}{\partial(\partial_j u)}\right] - \frac{\partial L}{\partial u} + \frac{\partial D}{\partial \dot{u}} = 0, \tag{48}$$

where u represents one of the components of vectors $\mathbf{u}$ and $\mathbf{U}^{(m)}$, $m = 1, 2$, taken here as generalized coordinates. The remaining equation regards the variable ζ,

$$\partial_t\left(\frac{\partial L}{\partial \dot{\zeta}}\right) - \frac{\partial L}{\partial \zeta} + \frac{\partial D}{\partial \dot{\zeta}} = 0. \tag{49}$$

We derive the following equations:

$$N\nabla^2\mathbf{u} + (A + N)\nabla e + Q_1\nabla(\xi_1 + \phi_2\zeta) + Q_2\nabla(\xi_2 - \phi_1\zeta)$$
$$= \rho_{00}\ddot{\mathbf{u}} + \sum_m\left[\rho_{0m}\ddot{\mathbf{U}}^{(m)} + b_m\left(\dot{\mathbf{u}} - \dot{\mathbf{U}}^{(m)}\right)\right],$$

$$Q_1\nabla e + R_1\nabla(\xi_1 + \phi_2\zeta) = \rho_{01}\ddot{\mathbf{u}} + \rho_{11}\ddot{\mathbf{U}}^{(1)} - b_1\left(\dot{\mathbf{u}} - \dot{\mathbf{U}}^{(1)}\right),$$

$$Q_2\nabla e + R_2\nabla(\xi_2 - \phi_1\zeta) = \rho_{02}\ddot{\mathbf{u}} + \rho_{22}\ddot{\mathbf{U}}^{(2)} - b_2\left(\dot{\mathbf{u}} - \dot{\mathbf{U}}^{(2)}\right),$$

$$\phi_2[Q_1 e + R_1(\xi_1 + \phi_2\zeta)] - \phi_1[Q_2 e + R_2(\xi_2 - \phi_1\zeta)]$$
$$= \frac{1}{3}R_0^2\phi_1^2\phi_2\phi_{20}\left(\frac{\rho_f}{\phi_{10}}\ddot{\zeta} + \frac{\eta}{\kappa_1}\dot{\zeta}\right). \tag{50}$$

This system of coupled equations has 10 unknowns $(u_i, U_i^{(m)}, i = 1, 2, 3, m = 1, 2,$ and $\zeta)$ and describes wave dispersion and attenuation due to the LFF process. There are six stiffnesses, $(A, N, Q_m$ and $R_m)$, five density coefficients $(\rho_{00}, \rho_{0m}$ and $\rho_{mm})$, three geometrical coefficients $(\phi_m$ and $R)$, the transport properties κ_m and the fluid viscosity η. The stiffness and density coefficients have been discussed in section 6. All these coefficients can be quantitatively estimated on the basis of some measurable properties of solid and fluid, so that this theory can easily be applied in practical problems.

8. Plane Wave Analysis

[36] We consider the plane wave kernel exp $i(\omega t - \mathbf{k} \cdot \mathbf{x})$, where ω is the angular frequency, $\mathbf{k}$ is the wave number

vector, and $i = \sqrt{-1}$. We assume homogeneous body waves; that is, the propagation and attenuation directions coincide. If $\mathbf{k} = \kappa - i\alpha$, where κ is the real wave number vector and α is the attenuation vector, then $\mathbf{k} = (\kappa - i\alpha)\hat{\kappa} = k\hat{\kappa}$, where $\hat{\kappa}$ defines the propagation (attenuation) direction, and k is the complex wave number. Following the procedure outlined in section 7.7 of *Carcione* [2007], i.e., substituting the plane wave kernel into equation (50), we obtain a cubic equation for P waves and one solution for S waves. The solutions yield the wave number k (see Appendix B).

[37] We then define the complex velocity

$$v = \frac{\omega}{k}, \tag{51}$$

such that

$$v_p = \left[\text{Re}\left(\frac{1}{v}\right)\right]^{-1}, \tag{52}$$

is the phase velocity,

$$\alpha = -\omega\text{Im}\left(\frac{1}{v}\right), \tag{53}$$

the attenuation factor, and

$$Q = \frac{\pi f}{\alpha v_p} = \frac{\text{Re}(v)}{2\text{Im}(v)} \tag{54}$$

is the quality factor, defined as the total energy (potential plus kinetic) divided by the dissipated energy [e.g., *Carcione*, 2007, equation (3.130)], where $f = \omega/(2\pi)$ is the frequency. The definition of Q as twice the potential energy divided by the dissipated energy $(Q = \text{Re}(v^2)/\text{Im}(v^2))$ may yield negative values for slow waves, since the LFF and Biot mechanisms are losses mainly associated with the kinetic energy rather than the strain energy [e.g., *Carcione*, 1998].

9. Examples

[38] In order to illustrate the results of the present theory, we use the same rock properties of *Pride and Berryman* [2003] to obtain the phase velocities and quality factors. The inclusion (phase 2) of radius R_0 is embedded in a host medium of radius $R_1 = 3R_0$, so that $v_1 = 0.963$ and $v_2 = 0.037$. The concentration of inclusions (0.037) in this example is much less than 0.2. The host medium in our model has a high volume ratio and constitutes the main phase. Then, the interactions between different inclusions can be neglected. The dry rock bulk moduli of the two phases are given by $K_{bm} = (1 - \phi_{m0})K_s/(1 + c_m\phi_{m0})$, where c_m are consolidation parameters, related to the Biot-Willis coefficients $\alpha_m = 1 - K_{bm}/K_s$ as $\alpha_m = (c_m + 1)\phi_{m0}/(1 + c_m\phi_{m0})$, and K_s is the grain bulk modulus. Moreover, $1/K_b = v_1/K_{b1} + v_2/K_{b2}$ and we assume that the composite shear modulus is given by $N = \mu_b = (1 - \phi)\mu_s/(1 + c_S\phi)$ where μ_s is the grain shear modulus and c_S is a shear consolidation parameter. We take $K_s = 38$ GPa, $\mu_s = 44$ GPa, $K_f = 2.5$ GPa, $\rho_s = 2650$ kg/m^3, $\rho_f = 1040$ kg/m^3, $\kappa_1 = 0.01$ D, $\kappa_2 = 1$ D, $\eta = 0.001$ Pa s (ambient water), $\eta = 0.005$ Pa s (oil), $\eta =$
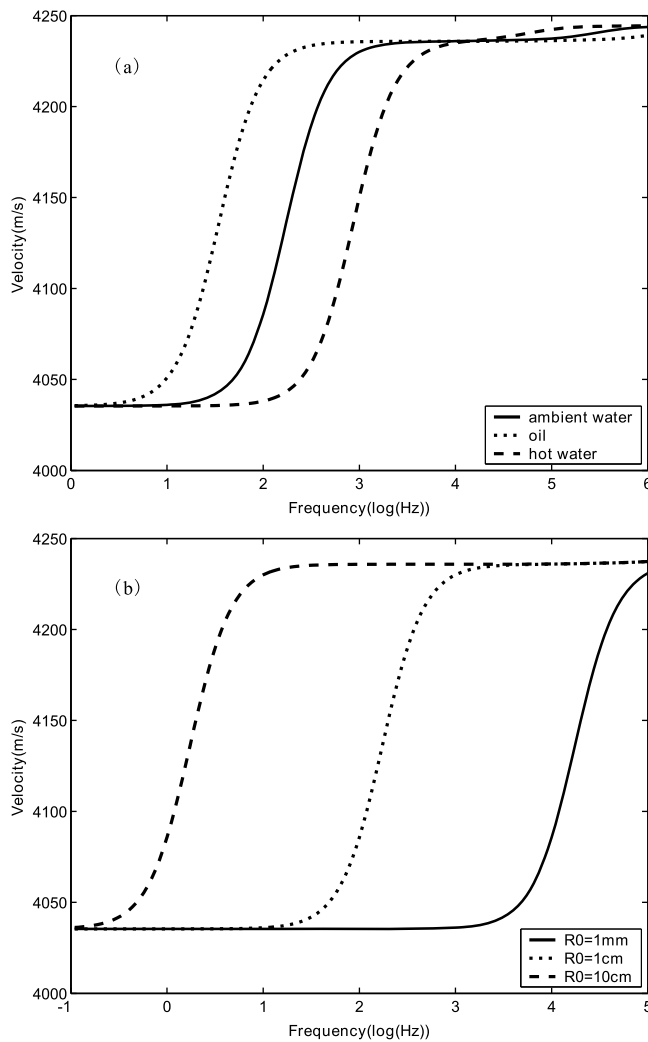
Figure 3. P wave phase velocities as a function of frequency for (a) different fluids and $R_0 = 1$ cm and (b) different radius of the inclusions and ambient water.

0.0002 Pa s (hot water), $\phi_{10} = 0.1$, $c_1 = 10$, $\phi_{20} = 0.3$, $c_2 = 200$, and $c_S = 10$.

[39] The phase velocity of the fast P wave (P1) as a function of frequency is shown in Figure 3. P1 velocities increase with wave frequency in seismic band. This low-frequency velocity dispersion of P1 is induced by mesoscopic LFF. Figure 4 displays the dissipation factor as a function of frequency for different fluids (Figure 4a) and different inclusion radii (Figure 4b). The results predicted by *Pride and Berryman.* [2003] are also shown. The smaller relaxation peak at the high frequencies represents the loss mechanism caused by Biot's friction [*Biot*, 1962]. The two theories show a similar qualitative behavior. The mesoscopic peaks are in the 1–1000 Hz range and the Q factor ranges from 15 to 30, typical of for reservoir rocks. Moreover, the LFF peaks move toward the low frequencies with increasing fluid viscosity and larger inclusion sizes. Higher attenuation is predicted by the present theory.

[40] *Pride et al* [2004] approximated the double-porosity equations by an effective single-porosity equation. Their theory does not predict slow P waves. In this study, the

velocity and attenuation of two slow P waves (P2 and P3) are estimated according to Appendix B. The wave velocities corresponding to the slow P waves and different fluids and inclusion radii are shown in Figures 5a and 5b, respectively. Figure 6 shows the corresponding dissipation factors. The P2 and P3 waves are diffusive modes at low frequencies, which are related to the fluid in the two components. The P2 and P3 velocities are approximately zero at the low frequencies (the diffusive regime), and increase with frequency. P2 inverse quality factors (dissipation factors) are around unity in zero frequency limit and decrease with frequency. The slow P wave diffusion is caused by viscous friction between the solid matrix and the pore fluid [*Biot*, 1956]. The differences in the P2 and P3 wave behavior arise from the different properties of the host medium and inclusions (porosity, permeability and matrix compressibility). The P3 dissipation factors increase with frequency in seismic band, which is caused by LFF. In ultrasonic band, P3 inverse quality factors decrease with frequency. At high frequencies, the fluid cannot relax and this state of unrelaxation induces pore pressure gradients.
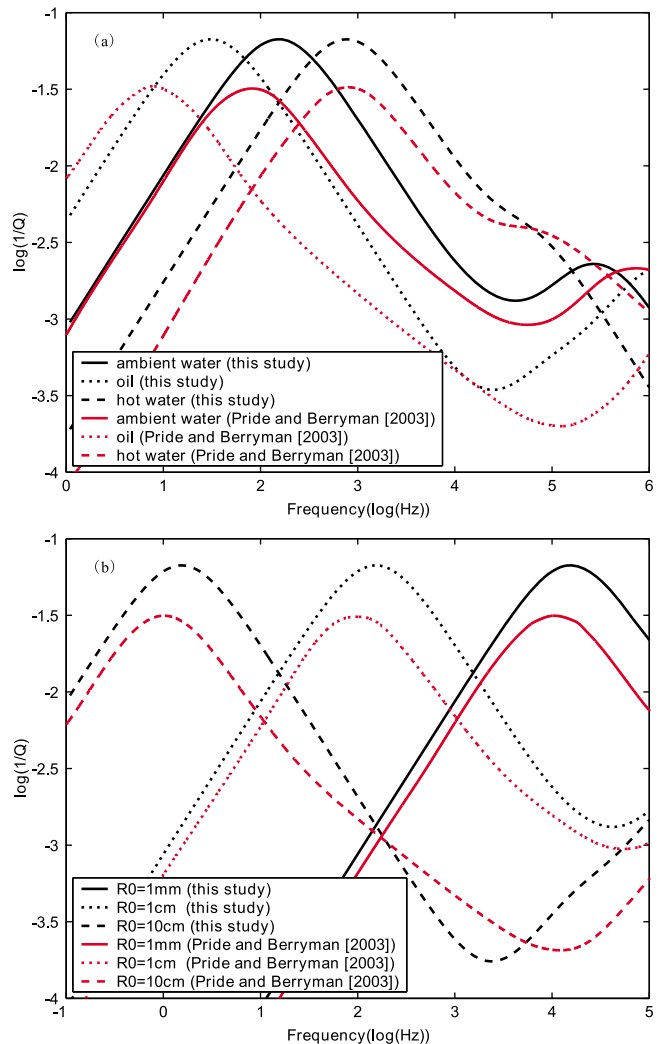

Figure 4. P wave dissipation factors as a function of frequency for (a) different fluids and $R_0 = 1$ cm and (b) different radius of the inclusions and ambient water.
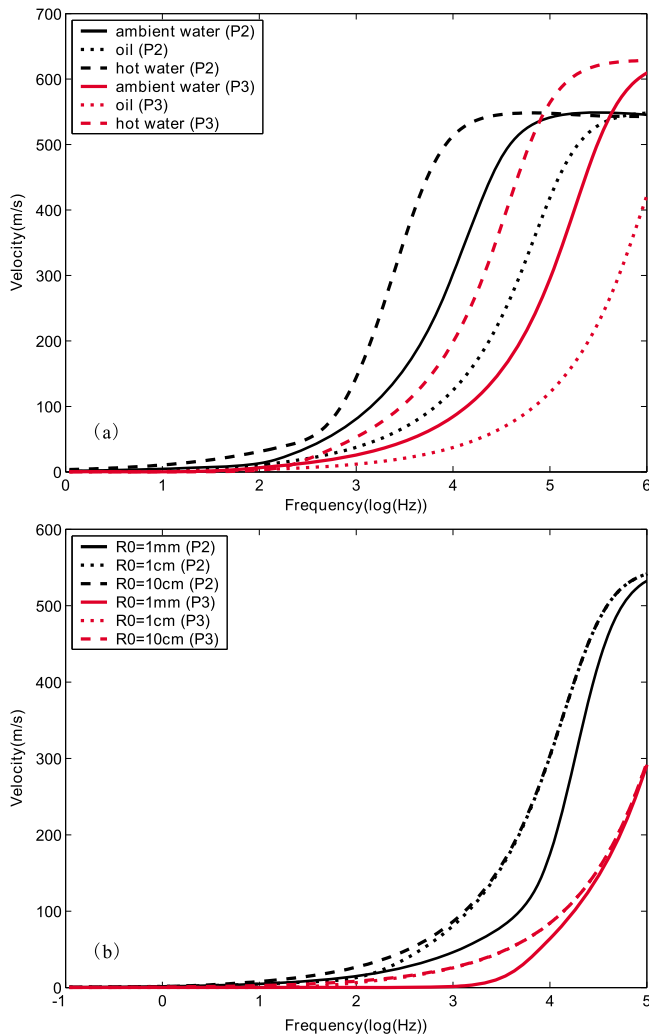
Figure 5. P2 and P3 wave phase velocities (black and red lines) as a function of frequency for (a) different fluids and $R_0 = 1$ cm and (b) different radii and ambient water.

local fluid flow causes fast P wave dispersion and attenuation in the 1–1000 Hz frequency band, for inclusion sizes between 1 mm and 10 cm. The local fluid flow peaks for fast P waves move toward low frequencies with increasing viscosity and/or larger inclusion size. The diffusion of the two types of slow P waves are mainly caused by the friction force between solid matrix and pore fluid in wave direction. There is slight dispersion and attenuation in ultrasonic band in S wave curves, which are also caused by Biot friction mechanism.

[43] The theory produced in this paper is only for isotropic double-porosity media. Because of the coupling between fluid motions and solid motion, which need not always be in phase, these result in three compressional waves (one fast P wave and two slow P waves), but only one possibly damped shear wave. In contrast, for anisotropic pure solid, we usually have two shear moduli. S waves with relatively lower speeds are also called "slow" S waves, nevertheless, these "slow" S waves are caused by wave polarization in anisotropic solid, and have nothing to do with solid-fluid

[41] Finally, the properties of the S wave are given in Figure 7. In this case, the curves are independent of the radii of the inclusions and the variations are mainly due to density effects. The attenuation peaks move to higher frequencies for increasing fluid viscosity. These features agree with the characteristics of Biot's friction. The attenuation is caused by the relative motion between the solid and the fluid.

10. Conclusions

[42] We have developed a double-porosity theory to describe wave propagation and mesoscopic attenuation in isotropic poroelastic media. The medium consists of spherical inclusions embedded in a host medium. The fluid flow induced by the wave motion is described by Rayleigh's theory of liquid collapse of a spherical cavity. The elastic coefficients are obtained by idealized ("gedanken") experiments and can be estimated from measurable quantities. In the numerical example for a sandstone, the theory predicts the usual fast P and S waves and two slow P modes. The
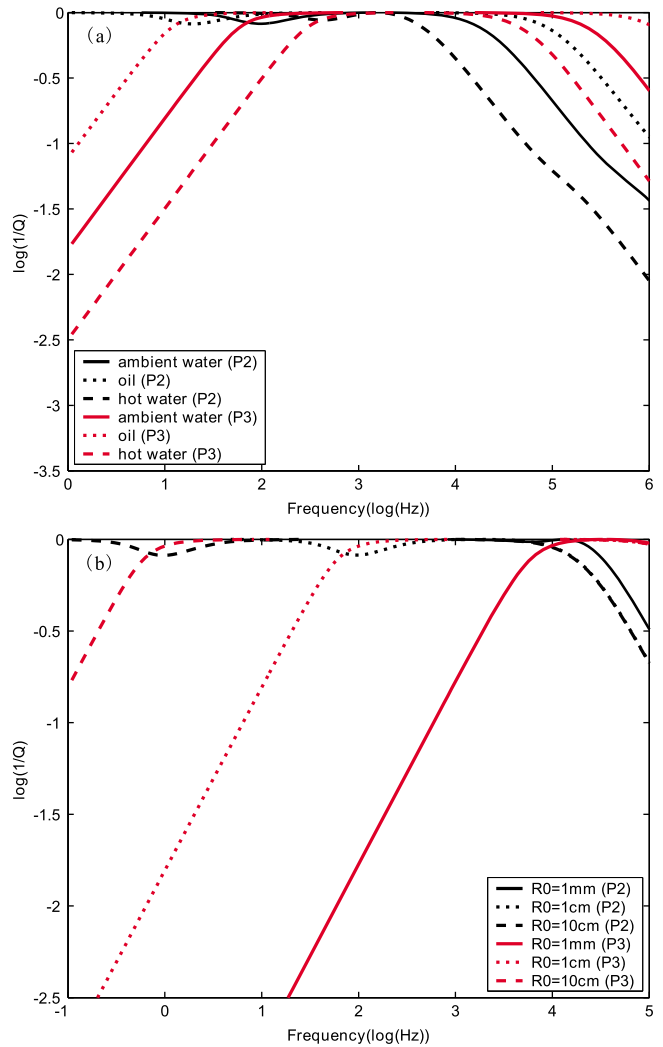

Figure 6. P2 and P3 wave dissipation factors (black and red lines) as a function of frequency for (a) different fluids and $R_0 = 1$ cm and (b) different radii and ambient water.
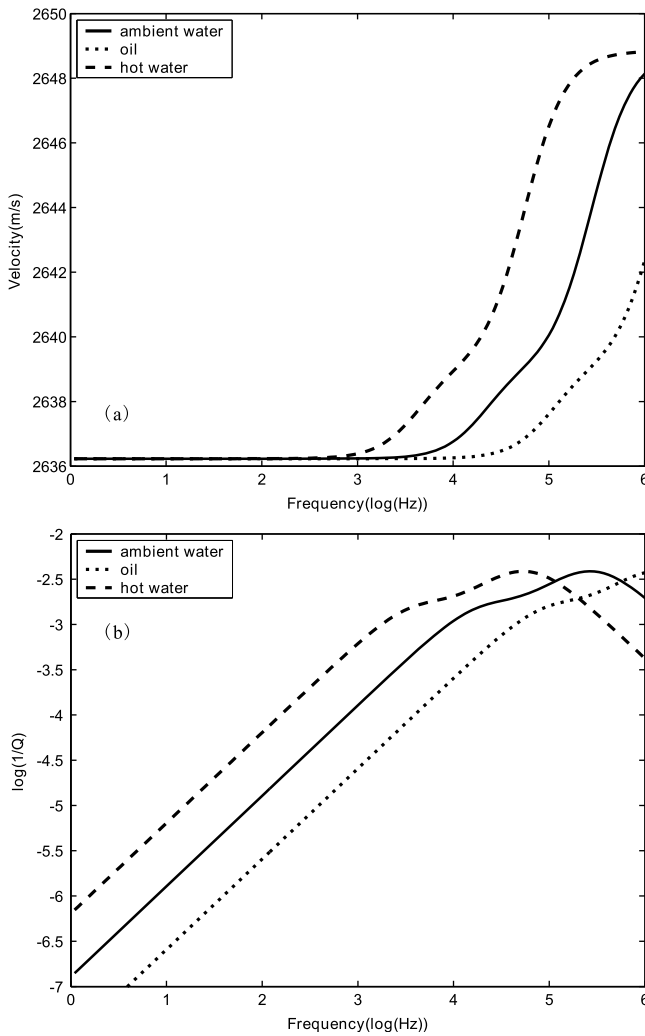
Figure 7. (a) S wave phase velocities and (b) dissipation factors as a function of frequency for different fluids.

coupling effect. This paper considers a single-fluid saturation and the case of attenuation for compressional waves. Partial fluid saturation and the case of shear losses due to local fluid flow will be studied in a future work.

Appendix A: Derivation of Equations (16) and (17)

[44] The components of the composite (inclusions and host medium) are assumed to be homogeneous and isotropic. Under an isostress squeezing generated by P waves (the P wavelength is assumed to be much larger than inclusion size), the local flow velocity vector $l_i^{(m)}$ has the same amplitude, l_R, at any coordinate on the sphere surface, and the oscillation direction of the local flow is perpendicular to the sphere's surface and radially oriented (see Figure A1a).

[45] To calculate the volume integral in a spherical coordinate system, we have

$$\int_{\Omega_m} l_i^{(m)} d\Omega_m = \int_0^{2\pi} d\theta_0 \int_0^\pi \sin\theta_1 d\theta_1 \int_0^{R_0} R^2 dR \cdot l_i^{(m)}. \quad (A1)$$

Since the local flow vector is radial from sphere center, as to a symmetrical sphere inclusion, in i direction we have

$$l_i^{(m)} = l_R \cos\theta_0 \cos\theta_1, \quad (A2)$$

where l_R is only relevant to sphere radius R, and independent to θ_0 and θ_1. Then

$$\int_{\Omega_m} l_i^{(m)} d\Omega_m = \int_0^{2\pi} \cos\theta_0 d\theta_0 \int_0^\pi \sin\theta_1 \cos\theta_1 d\theta_1 \int_0^{R_0} l_R R^2 dR, \quad (A3)$$

which is identical to zero. Thus equation (16) is derived.

[46] The components $g_i^{(m)}$ correspond to the fluid relative velocity associated with global fluid flow and cannot be put outside of the integral.

$$\int_{\Omega_m} g_i^{(m)} l_i^{(m)} d\Omega_m = \int_0^{2\pi} d\theta_0 \int_0^\pi \sin\theta_1 d\theta_1 \int_0^{R_0} R^2 dR \cdot g_i^{(m)} l_i^{(m)}. \quad (A4)$$
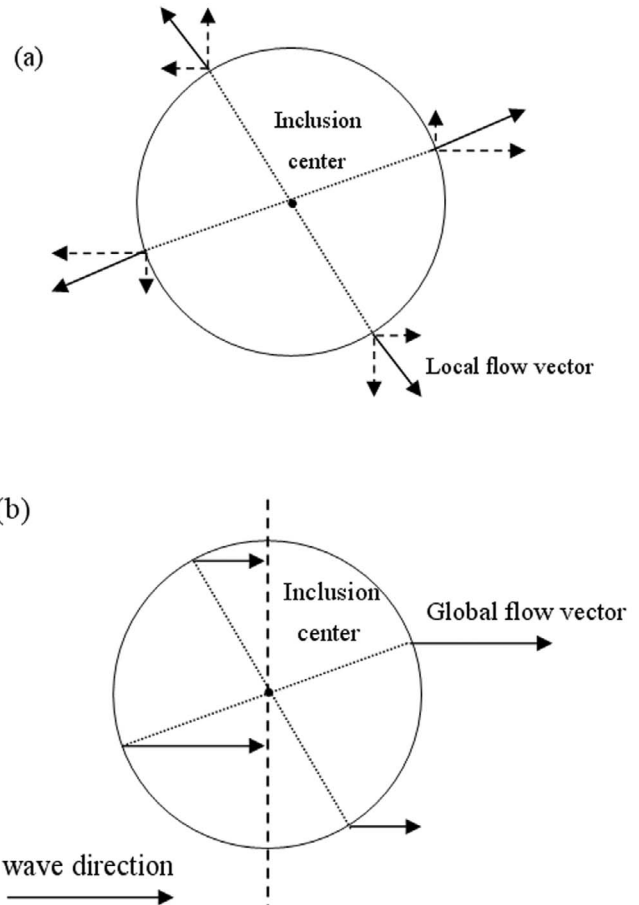

Figure A1. The axial sections of the sphere inclusion (the axis is parallel to the wave direction). (a) The velocity vectors of local fluid flow. (b) The velocity vectors of global fluid flow.

In i direction we have

$$l_i^{(m)} = l_R \cos\theta_0 \cos\theta_1. \tag{A5}$$

For plane waves, fluid vibration of global flow only happens in the wave propagation direction. Thus, we separate the sphere into two parts in the integral calculation. (See dashed line in Figure A1b, which crosses the sphere center and is perpendicular to the wave direction. The plane through this dashed line and perpendicular to the wave direction will cut the sphere into two halves.) So we have

$$
\begin{aligned}
\int_{\Omega_m} g_i^{(m)} l_i^{(m)} d\Omega_m &= \int_0^{2\pi} \cos\theta_0 d\theta_0 \int_0^{\pi} \sin\theta_1 \cos\theta_1 d\theta_1 \int_0^{R_0} l_R R^2 dR \cdot g_i^{(m)} \\
&= \int_0^{\pi} \cos\theta_0 d\theta_0 \int_0^{\pi} \sin\theta_1 \cos\theta_1 d\theta_1 \int_0^{R_0} l_R R^2 dR \cdot g_i^{(m)} \\
&\quad + \int_{\pi}^{2\pi} \cos\theta_0 d\theta_0 \int_0^{\pi} \sin\theta_1 \cos\theta_1 d\theta_1 \int_0^{R_0} l_R R^2 dR \cdot g_i^{(m)}.
\end{aligned}
\tag{A6}
$$

[47] Then, the second term on the right-hand side of the equality becomes

$$
\begin{aligned}
&\int_{\pi}^{2\pi} \cos\theta_0 d\theta_0 \int_0^{\pi} \sin\theta_1 \cos\theta_1 d\theta_1 \int_0^{R_0} l_R R^2 dR \cdot \left[g_i^{(m)}(\theta_0) \right] \\
&= \int_0^{\pi} \cos(\theta_0 + \pi) d(\theta_0 + \pi) \int_0^{\pi} \sin\theta_1 \cos\theta_1 d\theta_1 \int_0^{R_0} l_R R^2 dR \\
&\quad \cdot \left[g_i^{(m)}(\theta_0 + \pi) \right] \\
&= -\int_0^{\pi} \cos\theta_0 d\theta_0 \int_0^{\pi} \sin\theta_1 \cos\theta_1 d\theta_1 \int_0^{R_0} l_R R^2 dR \\
&\quad \cdot \left[g_i^{(m)}(\theta_0 + \pi) \right].
\end{aligned}
\tag{A7}
$$

For the symmetrical sphere inclusion, since the wavelength is much larger than the inclusion, we have

$$\left[g_i^{(m)}(\theta_0 + \pi) \right] = \left[g_i^{(m)}(\theta_0) \right] \tag{A8}$$

in the global flow along wave propagation direction.

[48] Then,

$$
\begin{aligned}
\int_{\Omega_m} g_i^{(m)} l_i^{(m)} d\Omega_m &= \int_0^{\pi} \cos\theta_0 d\theta_0 \int_0^{\pi} \sin\theta_1 \cos\theta_1 d\theta_1 \int_0^{R_0} l_R R^2 dR \\
&\quad \cdot g_i^{(m)} - \int_0^{\pi} \cos\theta_0 d\theta_0 \int_0^{\pi} \sin\theta_1 \cos\theta_1 d\theta_1 \\
&\quad \cdot \int_0^{R_0} l_R R^2 dR \cdot g_i^m = 0,
\end{aligned}
\tag{A9}
$$

then equation (17) is derived.

Appendix B: Solutions of Motion Equations

[49] Substituting the plane wave solution of P waves into (50), we find the equations for the P waves

$$
\begin{vmatrix}
a_{11}k^2 + b_{11} & a_{12}k^2 + b_{12} & a_{13}k^2 + b_{13} \\
a_{21}k^2 + b_{21} & a_{22}k^2 + b_{22} & a_{23}k^2 + b_{23} \\
a_{31}k^2 + b_{31} & a_{32}k^2 + b_{32} & a_{33}k^2 + b_{33}
\end{vmatrix} = 0,
\tag{B1}
$$

where

$$
\begin{aligned}
&a_{11} = P + \mathrm{i}(Q_2\phi_1 - Q_1\phi_2)q_1, & &a_{12} = Q_1 + \mathrm{i}(Q_2\phi_1 - Q_1\phi_2)q_2 & &a_{13} = Q_2 + \mathrm{i}(Q_2\phi_1 - Q_1\phi_2)q_3, \\
&a_{21} = Q_1 - \mathrm{i}R_1\phi_2 q_1, & &a_{22} = R_1(1 - \mathrm{i}\phi_2 q_2), & &a_{23} = -\mathrm{i}R_1\phi_2 q_3, \\
&a_{31} = Q_2 + \mathrm{i}R_2\phi_1 q_1, & &a_{32} = \mathrm{i}R_2\phi_1 q_2, & &a_{33} = R_2(1 + \mathrm{i}\phi_1 q_3), \\
&b_{11} = -\rho_{00}\omega^2 + \mathrm{i}\omega(b_1 + b_2), & &b_{12} = -\omega(\rho_{01}\omega + \mathrm{i}b_1), & &b_{13} = -\omega(\rho_{02}\omega + \mathrm{i}b_2), \\
&b_{21} = b_{12}, & &b_{22} = \omega(-\rho_{11}\omega + \mathrm{i}b_1), & &b_{23} = 0, \\
&b_{31} = b_{13}, & &b_{32} = 0, & &b_{33} = \omega(-\rho_{22}\omega + \mathrm{i}b_2),
\end{aligned}
\tag{B2}
$$

$P = A + 2N$, and

$$
\begin{aligned}
q_1 &= \mathrm{i}(\phi_2 Q_1 - \phi_1 Q_2)/S, \\
q_2 &= \mathrm{i}\phi_2 R_1/S, \\
q_3 &= -\mathrm{i}\phi_1 R_2/S, \\
S &= \tfrac{1}{3}\omega\phi_1^2\phi_2\phi_{20}R_0^2 \left(\frac{\mathrm{i}\eta}{\kappa_1} - \frac{\omega\rho_f}{\phi_{10}} \right) - \left(\phi_2^2 R_1 + \phi_1^2 R_2 \right).
\end{aligned}
\tag{B3}
$$

Equation (A1) gives three roots, corresponding to a fast P wave and two slow P waves denoted by P2 and P3.

[50] Similarly, substituting the plane wave solution of S wave into (50), we obtain the equation for the S wave as

$$N\frac{k^2}{\omega^2} = \rho_{00} + \frac{b_1 + b_2}{\mathrm{i}\omega} - \frac{\left(\rho_{01} - \frac{b_1}{\mathrm{i}\omega}\right)^2}{\rho_{11} + \frac{b_1}{\mathrm{i}\omega}} - \frac{\left(\rho_{02} - \frac{b_2}{\mathrm{i}\omega}\right)^2}{\rho_{22} + \frac{b_2}{\mathrm{i}\omega}}. \tag{B4}$$

The limit of the classical Biot theory is obtained for $\phi_{10} = \phi_{20} = \phi$ and $\kappa_1 = \kappa_2$. In this case the matrix is the same for the host medium and the inclusions, since $\phi_1 + \phi_2 = \phi_{10}v_1 + \phi_{20}v_2 = \phi$, because $v_1 + v_2 = 1$; Moreover $\mathcal{T}_1 = \mathcal{T}_2$ and $b_1 = b_2$.

References

Achenbach, J. D. (1984), *Wave Propagation in Elastic Solids*, North Holland, New York.
Agersborg, R., T. A. Johansen, and M. Jakobsen (2009), Velocity variations in carbonate rocks due to dual porosity and wave-induced fluid flow, *Geophys. Prospect.*, *57*, 81–98.
Ba, J., J.-X. Nie, H. Cao, and H.-Z. Yang (2008a), Mesoscopic fluid flow simulation in double-porosity rocks, *Geophys. Res. Lett.*, *35*, L04303, doi:10.1029/2007GL032429.
Ba, J., H. Cao, F. C. Yao, J.-X. Nie, and H.-Z. Yang (2008b), Double-porosity rock model and squirt flow in laboratory frequency band, *Appl. Geophys.*, *5*, 261–276.
Berryman, J. G. (1979), Theory of elastic properties of composite-materials, *Appl. Phys. Lett.*, *35*, 856–858.
Berryman, J. G., and P. A. Berge (1996), Critique of two explicit schemes for estimating elastic properties of multiphase composites, *Mech. Mater.*, *22*, 149–164.

Berryman, J. G., and H. F. Wang (2000), Elastic wave propagation and attenuation in a double-porosity dual-permeability medium, *Int. J. Rock Mech. Min. Sci.*, *37*, 63–78.

Biot, M. A. (1956), Theory of propagation of elastic waves in a saturated porous solid, I, Low-frequency range, *J. Acoust. Soc. Am.*, *28*, 168–178.

Biot, M. A. (1962), Mechanics of deformation and acoustic propagation in porous media, *J. Appl. Phys.*, *33*, 1482–1498.

Biot, M. A., and D. G. Willis (1957), The elastic coefficients of the theory of consolidation, *J. Appl. Mech.*, *24*, 594–601.

Brajanovski, M., T. M. Müller, and B. Gurevich (2006), Characteristic frequencies of seismic attenuation due to wave-induced fluid flow in fractured porous media, *Geophys. J. Int.*, *166*, 574–578.

Cadoret, T., D. Marion, and B. Zinszner (1995), Influence of frequency and fluid distribution on elastic wave velocities in partially saturated limestones, *J. Geophys. Res.*, *100*, 9789–9803.

Carcione, J. M. (1998), Viscoelastic effective rheologies for modeling wave propagation in porous media, *Geophys. Prospect.*, *46*, 249–270.

Carcione, J. M. (2007), *Wave Fields in Real Media: Theory and Numerical Simulation of Wave Propagation in Anisotropic, Anelastic, Porous and Electromagnetic Media*, 2nd ed., Elsevier Sci., Amsterdam.

Carcione, J. M., and S. Picotti (2006), P-wave seismic attenuation by slow-wave diffusion. Effects of inhomogeneous rock properties, *Geophysics*, *71*, O1–O8.

Carcione, J. M., and G. Seriani (2001), Wave simulation in frozen porous media, *J. Comput. Phys.*, *170*, 676–695.

Carcione, J. M., B. Gurevich, and F. Cavallini (2000), A generalized Biot-Gassmann model for the acoustic properties of shaley sandstones, *Geophys. Prospect.*, *48*, 539–557.

Carcione, J. M., H. B. Helle, and N. H. Pham (2003), White's model for wave propagation in partially saturated rocks: Comparison with poroelastic numerical experiments, *Geophysics*, *68*, 1389–1398.

Carcione, J. M., F. Cavallini, J. E. Santos, C. L. Ravazzoli, and P. M. Gauzellino (2004), Wave propagation in partially-saturated porous media: Simulation of a second slow wave, *Wave Motion*, *39*, 227–240.

Deresiewicz, H., and R. Skalak (1963), On uniqueness in dynamic poroelasticity, *Bull. Seismol. Soc. Am.*, *53*, 783–788.

Dutta, N. C., and H. Odé (1979a), Attenuation and dispersion of compressional waves in fluid-filled porous rocks with partial gas saturation (White model) – Part I: Biot theory, *Geophysics*, *44*, 1777–1788.

Dutta, N. C., and H. Odé (1979b), Attenuation and dispersion of compressional waves in fluid-filled porous rocks with partial gas saturation (White model) – Part II: Results, *Geophysics*, *44*, 1789–1805.

Dvorkin, J., and A. Nur (1993), Dynamic poroelasticity: A unified model with the squirt and the Biot mechanisms, *Geophysics*, *58*, 524–533.

Dvorkin, J., G. Mavko, and A. Nur (1995), Squirt flow in fully saturated rocks, *Geophysics*, *60*, 97–107.

Gurevich, B., V. B. Zyrianov, and S. L. Lopatnikov (1997), Seismic attenuation in finely layered porous rocks: Effects of fluid flow and scattering, *Geophysics*, *62*, 319–324.

Helle, H. B., N. H. Pham, and J. M. Carcione (2003), Velocity and attenuation in partially saturated rocks—Poroelastic numerical experiments, *Geophys. Prospect.*, *51*, 551–566.

Johnson, D. L. (1986), Recent developments in the acoustic properties of porous media, *Frontiers in Physical Acoustics XCIII*, edited by D. Sette, pp. 255–290, Elsevier, New York.

Johnson, D. L. (2001), Theory of frequency dependent acoustics in patchy-saturated porous media, *J. Acoust. Soc. Am.*, *110*, 682–694.

Knight, R., and R. Nolen-Hoeksema (1990), A laboratory study of the dependence of elastic wave velocities on pore scale fluid distribution, *Geophys. Res. Lett.*, *17*, 1529–1532.

Kuster, G. T., and M. N. Toksoz (1974), Velocity and attenuation of seismic waves in two-phase media: I. Theoretical formulation, *Geophysics*, *39*, 587–606.

Lamb, H. (1923), The early stages of a submarine explosion, *Philos. Mag.*, *45*, 257–265.

Liu, X., S. Greenhalgh, and B. Zhou (2009), Transient solution for poro-viscoacoustic wave propagation in double porosity media and its limitations, *Geophys. J. Int.*, *178*, 375–393.

Miksis, M. J. (1988), Effects of contact line movement on the dissipation of waves in partially saturated rocks, *J. Geophys. Res.*, *93*(B6), 6624–6634.

Müller, T. M., and B. Gurevich (2004), One-dimensional random patchy saturation model for velocity and attenuation in porous rocks, *Geophysics*, *69*, 1166–1172.

Murphy, W. F. (1982), Effects of microstructure and pore fluids on the acoustic properties of granular sedimentary materials, Ph.D. dissertation, Stanford Univ., Stanford, Calif.

Pride, S. R., and J. G. Berryman (2003), Linear dynamics of double-porosity and dual permeability materials. I. Governing equations and acoustic attenuation, *Phys. Rev. E*, *68*, 036603, doi:10.1103/PhysRevE.68.036603.

Pride, S. R., J. G. Berryman, and J. M. Harris (2004), Seismic attenuation due to wave-induced flow, *J. Geophys. Res.*, *109*, B01201, doi:10.1029/2003JB002639.

Rayleigh, L. (1917), On the pressure developed in a liquid during the collapse of a spherical cavity, *Philos. Mag.*, *34*, 94–98.

Santos, J. E, J. M. Corbero, and J. Douglas Jr. (1990a), Static and dynamic behavior of a porous solid saturated by a two-phase fluid, *J. Acoust. Soc. Am.*, *87*, 1428–1438.

Santos, J. E., J. Douglas Jr., J. M. Corbero, and O. M. Lovera (1990b), A model for wave propagation in a porous medium saturated by a two-phase fluid, *J. Acoust. Soc. Am.*, *87*, 1439–1448.

Santos, J. E., C. L. Ravazzoli, and J. M. Carcione (2004), A model for wave propagation in a composite solid matrix saturated by a single-phase fluid, *J. Acoust. Soc. Am.*, *115*, 2749–2760.

Shapiro, S. A., and T. M. Müller (1999), Seismic signatures of permeability in heterogeneous porous media, *Geophysics*, *64*, 99–103.

Vokurka, K. (1985a), On Rayleigh's model of a freely oscillating bubble. I. Basic relations, *Czech. J. Phys.*, *35*(1), 28–40.

Vokurka, K. (1985b), On Rayleigh's model of a freely oscillating bubble. II. Results, *Czech. J. Phys.*, *35*(2), 110–120.

White, J. E. (1975), Computed seismic speeds and attenuation in rocks with partial gas saturation, *Geophysics*, *40*, 224–232.

White, J. E., N. G. Mikhaylova, and F. M. Lyakhovitskiy (1975), Low-frequency seismic waves in fluid saturated layered rocks, *Izv. Acad. Sci. USSR Phys. Solid Earth*, *11*, 654–659.

Wilkens, R. H., G. J. Fryer, and J. Karsten (1991), Evolution of porosity and seismic structure of upper oceanic crust: Importance of aspect ratios, *J. Geophys. Res.*, *96*, 17,981–17,995.

J. Ba, Department of Geophysics, RIPED, PetroChina, Xueyuan Rd. 20, 100083, Beijing, China. (baj04@mails.tsinghua.edu.cn)

J. M. Carcione, Istituto Nazionale di Oceanografia e di Geofisica Sperimentale, Borgo Grotta Gigante 42c, I-34010 Sgonico, Trieste, Italy.

J. X. Nie, State Key Laboratory of Exploration Science and Technology, Beijing Institute of Technology, 100081, Beijing, China.